Performance Comparison of Interaction Control Strategies on a Hand Rehabilitation Robot

Jean-Claude Metzger, Olivier Lambercy and Roger Gassert
Rehabilitation Engineering Laboratory, ETH Zurich, Leonhardstrasse 27, CH-8092 Zurich, Switzerland
Email: {jemetzge, olambercy, gassertr}@ethz.ch

***Abstract*—Numerous upper-limb rehabilitation robots have been developed to complement physical therapy following stroke. Most systems have focused on providing passive or assisted movement therapy, largely neglecting the haptic aspects of interaction with the environment. We argue that, especially for the training of object manipulation, rehabilitation robots should be able to stably render a broad dynamic range of impedances. Furthermore, the apparent dynamics of a rehabilitation robot might alter the motion of a patient or impact assessments performed with the device, and should therefore be characterized in detail. We implemented and compared different interaction controllers on a hand rehabilitation robot, the ReHapticKnob, and characterized the dynamic performance using conventional performance metrics as well as with a human in the loop. We further propose transparency planes, an extension to the regression of interaction data proposed in the literature, as a simple performance metric allowing a visual appreciation and comparison of the apparent dynamics of a device in transparency mode. Impedance control with force feedback outperformed the other control schemes and achieved a dynamic impedance range of 82 dB at 0.5 Hz and 35 dB at 10 Hz along the linear degree of freedom of the ReHapticKnob. The implications of these results are discussed in the context of robot-assisted assessment and therapy.**

I. INTRODUCTION

Over the past decades, a number of robotic systems have been developed to complement physical therapy following stroke and other neurological injuries, by assisting patients' movements and increasing intensity and duration of therapy [1]. Ideally, a rehabilitation robot should be able to cope with different impairment levels, always providing the right amount of support and challenge to the patient [2]. On the one hand, severely impaired stroke patients with very limited remaining motor function will require support from the robot to perform passive movements, while the patient's limb may even resist motion due to increased muscle tone or tendon reflex activity. Accordingly, the robotic system must provide stiff but stable guidance [3]. On the other hand, fine-motor skill training in moderately to mildly impaired patients, as well as performing robotic assessments, require the robot to render a wide range of dynamic interaction, all the way to full transparency. Minimizing residual interaction forces (i.e. rendering transparency) is crucial to assure that the motor commands generated by the patient and the resulting dynamics are captured without being masked or altered by the robot dynamics [4], [5]. Exploring the parameter space between transparency and stiff guidance is especially important for robotic devices targeting hand rehabilitation, where typical exercises are based on the training of activities of daily living (ADL), such as grasping and manipulation of objects with different mechanical properties [6]. This scenario requires robots capable of rendering rigid contact, i.e., sudden transitions from minimal (transparency) to maximal (rigid object) output impedance, or anywhere in between. Therefore, a rehabilitation robot should be able to cope with these contradictory control scenarios, i.e., rendering low and high impedance as well as stable transitions from the one to the other extreme. A broad renderable impedance range (Z-width) [7] has already been identified as a requirement for rehabilitation robots, with several works attempting to achieve this on state-of-the-art upper limb (e.g. MEMOS [2], InMotion [5], MIT-Manus [8] or MAHI Exo 1 [9]) and lower limb (e.g. the LOPES [10] or the Lokomat [11]) devices.

Besides the very limited number of devices dedicated to hand therapy presented to date, many of the existing robotic rehabilitation systems neglect haptic aspects of object manipulation. Typically, they are either limited in their maximal applicable output force, which limits the ability to simulate variable mechanical object properties or to passively guide severely impaired patients [12], [9] or they suffer from relatively high output impedance, limiting their ability to render transparency [13].

We have developed the ReHapticKnob, an end-effector based high-fidelity rehabilitation robot to train and assess hand function in stoke survivors, specifically grasping function and forearm pronation/supination [14], [15]. In this paper, we aim at characterizing performance of the linear grasping DOF of the device under different interaction control schemes, namely impedance control (ImpC) with force feedback [16], [17] and admittance control (AdmC) [16], [18], and maximizing the quality of the dynamic physical interaction that can be achieved for rehabilitation applications. Conventional haptic performance metrics [19], [7], [20] are used to characterize the dynamic behavior of the device, complemented by *transparency planes*, an extension of the regressions presented in [5] based on measured human-in-the-loop interaction data. Performance results are discussed with respect to their implications for robot-assisted rehabilitation.

In the following sections, scalars are denoted in normal font (e.g. q_1, f_{ee}, τ_z), vectors in small bold letters (e.g. $\boldsymbol{q} = [q_1, q_2]^\mathsf{T}$, $\boldsymbol{f}_{user} = [f_{ee}, \tau_z]^\mathsf{T}$) and matrices in capital bold letters (e.g. $\boldsymbol{K}_f = diag(k_f, k_\tau)$). A superscript j before a variable indicates the joint space representation, e.g. ${}^j\boldsymbol{Z}_{RHK}$.

978-1-4799-1808-9/15/$31.00

II. Interaction Control

The ReHapticKnob (RHK) is a two-degrees-of-freedom (DOF) hand rehabilitation device conceived for assessment and therapy of hand function in stroke patients. It follows an end-effector based design concept as shown in Figure 1. Both DOF are independently actuated by two motor-gear combinations. The translational DOF can open and close the hand, i.e., guide or resist grasping movements, with two mechanically-coupled finger supports moving in opposing direction, with motion transmitted from a geared motor to two belt transmissions via a pulley. The thumb and fingers can be fixed with Velcro straps to the finger supports, such that active hand opening can also be trained. The design is presented in detail in [14].

The RHK, as most rehabilitation robots, is back-drivable but cannot be classified as a low-output-impedance device such as the Phantom Omni [21]. Moving the output of the uncontrolled device along the translational DOF requires forces of over 6 N due to inherent friction and the reflected inertias of the motor/gear combination. Therefore, a simple ImpC [22] that renders a desired impedance $\boldsymbol{Z}_d$ on top of the inherent impedance of the RHK $\boldsymbol{Z}_{RHK}$ – such that the apparent impedance becomes $\boldsymbol{Z}_{app} = \boldsymbol{Z}_d + \boldsymbol{Z}_{RHK}$ – may not be suitable for neurologically impaired patients with reduced motor function (e.g. due to muscle weakness) or to train fine motor skills.

To achieve a transparent behavior ($\boldsymbol{Z}_{app} \rightarrow 0$) with an ImpC scheme, a force feedback (explicit force control) can be implemented to compensate for the device dynamics [16], [17]. The implementation of an AdmC scheme [16], [18], [23] is another possibility to enable interaction with a human user by enforcing the desired output dynamics through an inner motion control loop (implicit force control).

These control schemes require a good velocity estimate for a smooth and stable rendering of velocity-dependent force fields and a direct measurement of the interaction force. The resolution of the velocity estimate is affected both by the sampling rate (higher sampling rate resulting in lower velocity resolution) and the spatial resolution of the position sensor [24]. In this work, both the Finite Difference Method (FDM) with Butterworth (BW) filter and the First Order Adaptive Windowing (FOAW) Estimator [24] were evaluated with the aim of maximizing the renderable impedance range of the RHK.

A. Impedance Control

An ImpC receives motion as input and outputs force [22]. Accordingly, to render transparency, a back-drivable device is required, either inherently or through control. To mask the output impedance of the RHK, a force feedback was implemented, which can, at least partially, compensate for the dynamic behavior of the device, as well as for nonlinear effects without the need for a model.

The implementation of the ImpC with force feedback on the RHK is described in [15].

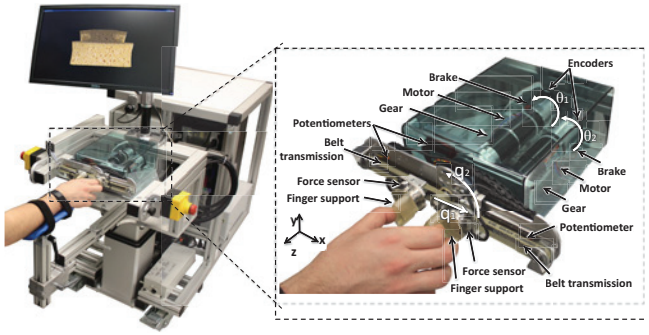

Fig. 1. The ReHapticKnob – a two DOF haptic device for the rehabilitation of hand function – shown while rendering a virtual object. The inlet shows a close-up view of the robotic system (actuation, sensing and mechanical transmission), with white arrows indicating the two DOF (translation and rotation) in task (q_1, q_2) and joint space coordinates (θ_1, θ_2).

B. Admittance Control

An admittance controller receives a force input and outputs motion in response [25], following the inverse concept of the ImpC. For this reason, a force sensor at the output of the device and an inner motion control loop to induce the desired motion at the end-effector are required.

The block diagram of the AdmC implemented on the RHK is shown in Figure 2, where an inner velocity control loop is realized with a stiff PD-controller on the joint-space velocity $\dot{\boldsymbol{\theta}}$ of the RHK. The measured force $\boldsymbol{f}_{meas}$ is used as input to the virtual admittance model (outer control loop) on the real-time system. Additionally, a feedforward of the measured force is fed directly into the inner control loop to compensate for the force applied by the user. This force feedforward is known to improve the dynamic behavior in position-based force control loops [18]. The inner control loop can also be closed around the position $\boldsymbol{q}$ instead of the velocity $\dot{\boldsymbol{q}}$. In this case, the virtual acceleration $\ddot{\boldsymbol{q}}_c$ has to be integrated twice to obtain a virtual position $\boldsymbol{q}_c$ which is then used in the inner position control loop as the desired variable.

The admittance model is based on two compensator blocks defined as $\boldsymbol{C}$ and $\boldsymbol{Z}_{virt}$. $\boldsymbol{C}$ is implemented as a virtual inertia $\boldsymbol{M}_c$ which is subject to virtual damping $\boldsymbol{B}_c$. $\boldsymbol{B}_c$ allows to decrease $\boldsymbol{M}_c$ such that transparency rendering and therefore the haptic interaction quality is improved. $\boldsymbol{M}_c$ is accelerated by the net difference of the measured interaction force $\boldsymbol{f}_{meas}$ and a virtual force $\boldsymbol{f}_{virt}$ (introduced below):

$$\boldsymbol{M}_c \cdot \ddot{\boldsymbol{q}}_c + \boldsymbol{B}_c \cdot \dot{\boldsymbol{q}}_c = \boldsymbol{f}_{meas} - \boldsymbol{f}_{virt} \tag{1}$$

$$\text{where} \quad \boldsymbol{M}_c = \begin{bmatrix} m_c & 0 \\ 0 & i_c \end{bmatrix} \quad \text{and} \quad \boldsymbol{B}_c = \begin{bmatrix} b_{c,1} & 0 \\ 0 & b_{c,2} \end{bmatrix}.$$

The second compensator block, $\boldsymbol{Z}_{virt}$, contains the implemented task-specific virtual impedance components (e.g. uni- or bidirectional spring-damper combinations), which result in a virtual force $\boldsymbol{f}_{virt}$ based on the input difference between a desired velocity $\dot{\boldsymbol{q}}_d$ and the virtual velocity $\dot{\boldsymbol{q}}_c$. Carignan and Cleary described the use of the actual motion (e.g. the

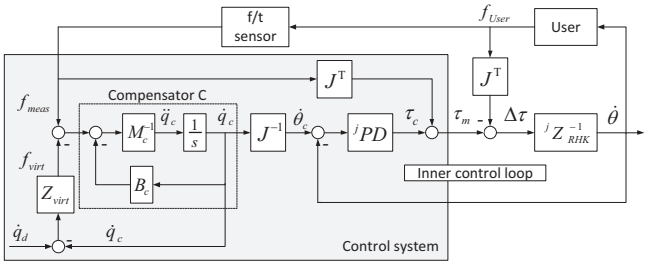

Fig. 2. Block diagram of the admittance control scheme with force feedforward, inner velocity control loop and virtual damping B_c.

measured position $\boldsymbol{q}$) of the robot as an input to the virtual admittance block $\boldsymbol{Z}_{virt}$ ("admittance control with position feedback") [16]. It can be argued that integrating the virtual motion (in the case of the RHK the virtual velocity $\dot{\boldsymbol{q}}_c$) will result in a biased virtual position $\boldsymbol{q}_c$, such that the output position and the virtual position can diverge over time. In contrast, differentiating and filtering the measured and thus noisy position feedback signal $\boldsymbol{q}$ will introduce a phase delay in the closed control loop and therefore lower the stability margin which then has to be compensated by, e.g., a larger virtual admittance $\boldsymbol{M}_c$. Hence, to increase the Z-width of the AdmC the virtual velocity $\dot{\boldsymbol{q}}_c$ was used as input to the compensator block $\boldsymbol{Z}_{virt}$. The interaction dynamics can be described based on the block diagram in Figure 2, by assuming high and therefore negligible force sensor dynamics ($\boldsymbol{f}_{meas} = \boldsymbol{f}_{user}$) and by setting, without loss of generality, $\dot{\boldsymbol{q}}_d = 0$:

$$[[\boldsymbol{M}_c \cdot s + \boldsymbol{B}_c] + \boldsymbol{Z}_{virt}] \cdot \dot{\boldsymbol{q}} = \boldsymbol{f}_{user} \tag{2}$$

The closed-loop stability of an admittance-controlled device depends on the phase margin of the closed-loop system while interacting with a user. The virtual inertia $\boldsymbol{M}_c$ adds a constant phase shift of $-90\ deg$ to the closed-loop system, independent of its value. Decreasing the virtual inertia $\boldsymbol{M}_c$ results in an increase of the feedback gain of the closed-loop system and can eventually destabilize the system. Virtual damping $\boldsymbol{B}_c$ reduces the phase shift of the closed-loop system at low frequencies, which are excited by the human-robot interaction. Hence, a minimal damping B_c increases the phase margin and contributes to the closed-loop stability.

III. Performance Evaluation

To characterize the dynamic performance of the RHK and compare the interaction controllers, a number of conventional performance metrics were determined. These include both the evaluation of the haptic system itself (in unpowered, powered and controlled conditions) based on metrics proposed in [19], [26], [27], as well as a characterization of the human-robot interaction quality [20], [15].

As an extension to the regression of interaction data proposed in [5], we further propose *transparency planes* as a simple metric to visually capture and compare the quality of the interaction control performance. Transparency planes are three dimensional plots allow a comparison of the lower apparent impedance boundaries of a haptic device based on human-robot interaction measurements, e.g., for the uncontrolled versus controlled behavior or between different interaction controllers. Compared to the Z-width, transparency planes do not require any transformations and do not rely on any theoretical assumptions.

Transparency planes are obtained by moving the end-effector by hand at different velocities during transparency rendering while interaction force f_{ee} and motion $\dot{q}$ are recorded at the output. Through multiple linear regression, a linear model ($m_{app} \cdot \ddot{q} + b_{app} \cdot \dot{q} = f_{ee}$) can then be fitted to force, velocity and acceleration recordings. m_{app} and b_{app} are the apparent inertia and damping felt by the user during human-robot interaction. The recordings (force-motion trajectory f_{ee}, $\ddot{q}_1$ and $\dot{q}_1$) and the model fit can then be plotted as points and as a plane, respectively, in a three-dimensional plot. x- and y-axes are scaled to the velocity and acceleration saturation limits of the device. Thereby, the recorded force-motion trajectory (point cloud) indicates to what extend the controller allows the user to exploit the achievable dynamics of the powered system. If the trajectory points lie close to the fitted plane, i.e., the residuals of the multiple linear regression fit are small, the assumed linearity of the transparency plane model can be validated.

A. Performance Measurements

The ImpC with force feedback and the AdmC with inner position and velocity control loop were implemented and evaluated. Table I summarizes conventional haptic metrics for the translational DOF of the RHK. The bandwidth and the phase margin of the position-controlled device were 7.9 Hz and 80 deg while a bandwidth of 9.6 Hz and a phase margin of 152 deg were identified for the velocity-controlled device. The Z-width plots and transparency planes resulting from human-robot interaction are presented in Figs. 3 and 4.

TABLE I
Performance characteristics of the ReHapticKnob, reported with respect to the end-effector. (m/i: mass/inertia)

Performance measure	Translational DOF
Range of motion	30-200 mm
Pos. resolution	0.0024 mm
Vel. resolution @1kHz	2.45 $\frac{mm}{s}$
F/T meas. in x,y (and z)	$\pm$80 N ($\pm$240 N)
Max. (cont.) act. force	1181 N (88 N)
Static friction	6 N
Structural stiffness	200 $\frac{kN}{m}$
Maximum vel. (acc.)	0.52 $\frac{m}{s}$ (13.25 $\frac{m}{s^2}$)
Closed-loop pos. / vel. BW	7.9 Hz / 9.6 Hz
Reflected motor m/i	24.5 kg
Uncontrolled / controlled m/i	32 kg / 0.8 kg
Uncontrolled / controlled damping	141 $\frac{N}{m/s}$ / 2.7 $\frac{N}{m/s}$
Inertial ratio	$2.05{\cdot}10^{-5} s^2$

1) Output Impedance and Z-width: The output impedance and Z-width plots of the translational DOF of the RHK are

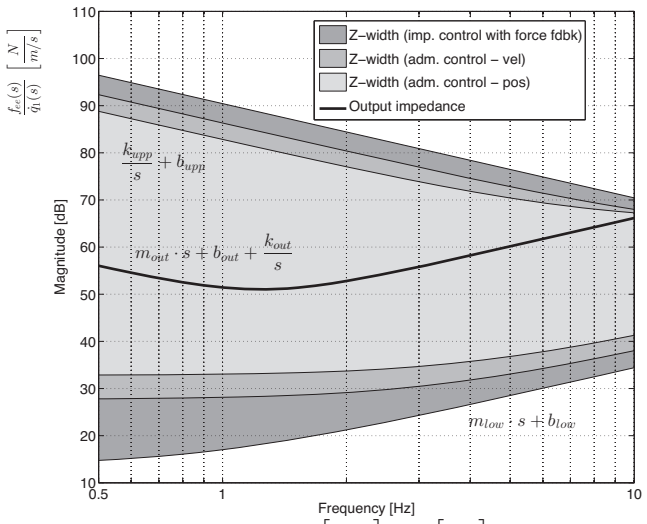

	m [kg]	b $\left[\frac{N}{m/s}\right]$	k $\left[\frac{kN}{m}\right]$	RMSE [dB]
ImpC - UB	-	1	209	7.0
AdmC - vel - UB	-	1'420	130	5.1
ImpC - pos - UB	-	1'850	86	5.0
Output impedance	32.3	356.4	1.9	2.8
AdmC - pos - LB	1.7	43.6	-	2.1
AdmC - vel - LB	1.2	24. 3	-	5.3
ImpC - fdbk - LB	0.8	4.8	-	3.5

Fig. 3. Output impedance of the ReHapticKnob (passive device dynamics) and renderable impedance range (Z-width) for the translational DOF: Z-width for AdmC with inner position control loop (light grey area), Z-width for AdmC with inner velocity control loop (medium grey area) and largest renderable impedance range for ImpC with force feedback (fdbk, dark grey area). A simple ImpC was used to render the upper Z-width boundaries. Force and motion data to estimate impedance were measured at the output. Values of the fitted parameters and the corresponding root mean square errors (RMSE) are indicated in the table. UB: upper bound, LB: lower bound.

plotted in Figure 3, in which a Z-width range comparison for impedance and admittance controllers is provided. The ImpC with force feedback was able to reduce the inherent damping and inertia of the device by 30–40 dB over the entire frequency range. A force feedback gain of $k_f = 16$ could be applied, such that the closed-loop system, i.e., the one with the human in the loop, remained stable.

The upper impedance curve $Z_{upp}(s)$ of the ImpC was achieved with a simple ImpC, i.e., without force feedback. A stiff spring-damper combination $Z_d = k_d/s + b_d$ with $k_d =$ 150 kN/m and $b_d = 150$ N/(m/s) could be rendered stably while perturbing the output. A maximum apparent stiffness of 209 kN/m was achieved at the output and allowed to increase the apparent impedance of the device by 40 dB at low frequencies, approaching the output impedance for frequencies above 10 Hz. For the ImpC with force feedback this resulted in an overall achievable dynamic impedance range of 82 dB at 0.5 Hz and 35 dB at 10 Hz.

The Z-width of the AdmC with inner velocity and position control loop is also plotted in Figure 3 in comparison to the ImpC. The two cases with different inner motion control loops required different values for the virtual damping to keep $m_c = 1$ kg. The AdmC with inner position control loop required a larger damping $b_{c,1} = 50$ N/(m/s) for a stable human-robot interaction while a smaller virtual damping of $b_{c,1} = 20$ N/(m/s) could be used for the AdmC with inner velocity control loop.

During upper impedance boundary rendering an infinite virtual mass m_c was selected such that any force applied by the user resulted in zero desired motion $\dot{\theta}_{c,1} = 0$. The spring-like behavior of the proportional control element of the inner position control loop was able to keep the actual position close to the desired position $\theta_1 \simeq \theta_{c,1}$. While rendering the same infinite virtual mass m_c with the inner velocity control loop the output could be moved as the velocity and not the position was controlled, i.e., the end-effector displacement (position error) was not controlled to zero. Thus, a smaller virtual mass $m_c = 5$ kg with an attached stiff virtual spring-damper element $Z_{virt} = k_{d,1}/s + b_{d,1}$ ($k_{d,1} = 60$ kN/m, $b_{d,1} =$ 3'000 N/(m/s)) resulted in the smallest positional deflections for the AdmC with inner velocity control loop. Thanks to the attached spring-damper element the output of the device was controlled back to the initial spring position after any small deviation. Both admittance controllers were able to reduce the apparent impedance during transparency rendering by 20–30 dB and increased the impedance by 30–40 dB during upper impedance boundary rendering at low frequencies, again approaching the output impedance (passive dynamics) of the RHK around 10 Hz. The dynamic impedance range achievable under AdmC with inner velocity loop was 64 dB at 0.5 Hz and 30 dB at 10 Hz. With an inner position control loop, a dynamic impedance range of 55 dB was achieved at 0.5 Hz and 26 dB at 10 Hz.

2) Transparency Planes: Transparency planes were derived for (i) the uncontrolled device, (ii) during transparency rendering under ImpC with force feedback, and (iii) during transparency rendering under AdmC with inner velocity control loop (Figure 4). For the uncontrolled device an apparent mass of 32 kg and an apparent damping of 141 N/(m/s) were identified. The ImpC with force feedback reduced the apparent mass by 97.5% (to 0.8 kg) and the damping by 98.1% (to 2.7 N/(m/s)) compared to the uncontrolled device. Dynamic human-robot interaction movements (large velocity and acceleration values) were recorded, surpassing the maximum velocity (v_{max}) and acceleration (a_{max}) of the actuated RHK. For the AdmC with inner velocity control loop, virtual admittance values of $m_c = 1$ kg and $b_{c,1} =$ 20 N/(m/s) were selected and the fitted apparent impedance parameters were identified as $m_c = 1.3$ kg and $b_{c,1} = 8.6$ N/(m/s), reflecting a reduction of 95.9% and 93.9% compared to the uncontrolled device, respectively.

IV. Discussion and Conclusions

We presented the detailed performance characterization of a hand rehabilitation robot under different interaction control schemes. Many devices currently used in robot-assisted rehabilitation lack high fidelity haptic rendering capabilities, especially at the level of the hand. Furthermore, a detailed performance characterization, including a discussion of how

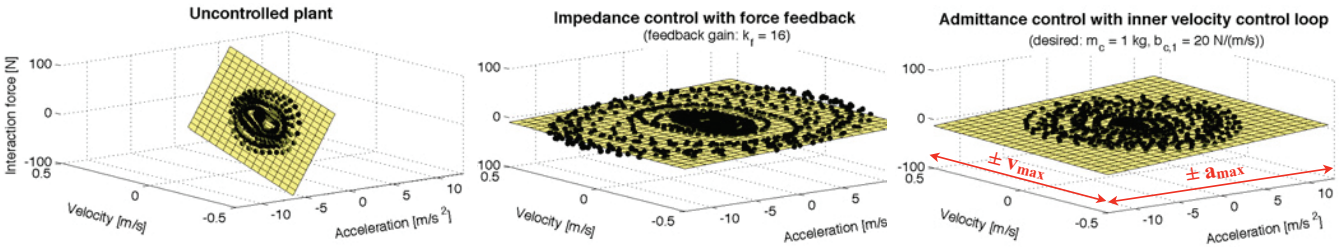

Fitting condition	m_{app} [kg]	b_{app} [N/(m/s)]	R^2	# fitted points	Max. residual [N]	Avg. residual [N]
Uncontrolled plant	32	141	0.96	10730	11.6	3.1
Impedance control with force feedback	0.8	2.7	0.99	10082	4.1	0.31
Admittance control	1.3	8.6	0.98	9826	3.3	0.43

Fig. 4. *Transparency planes:* user experienced transparency (apparent dynamics) during physical human-robot interaction with different control approaches: uncontrolled device, ImpC with force feedback and AdmC with inner velocity control loop. Recorded force-motion trajectories (black dots) are plotted over velocity and acceleration to indicate the damping and inertia components of the apparent impedance. A linear fit (yellow plane) and the identified model parameters of the apparent damping b_{app} and mass m_{app} (table) allow a qualitative and quantitative comparison between the performance of the different control approaches. The goodness of fit (R^2), the number of fitted points, as well as the maximum and the averaged absolute residuals as reported in the table indicate the fitting accuracy of the transparency planes.

the apparent device dynamics could mask or alter patients' movements or sensorimotor assessments, is rarely provided. The ReHapticKnob characterized in this paper can modulate the output impedance from high transparency, critical for the assessment of both motor and sensory function, provide various levels of assistance/resistance all the way up to passive guidance, and allows dynamic interaction with a variety of virtual objects while precisely assessing interaction forces and motion.

A. Comparison of the Interaction Controllers

The largest renderable impedance range was achieved by the ImpC with force feedback, which outperformed the AdmC, both with inner velocity and inner position control loop. The performance of the admittance controllers during transparency rendering was mainly limited by the bandwidth of the inner control loops.

During upper impedance boundary rendering a stiffness dominated behavior could be observed for almost the entire fitted frequency range. This is explained by the strong proportional position control action (large virtual stiffness K of the ImpC and the AdmC with inner velocity control loop or large proportional control gain P of the AdmC with inner position control loop). The upper impedance curve of the AdmC with inner position control loop could theoretically reach the same impedance level as the ImpC as both employ a similar control action. The increased upper impedance boundary of the ImpC is renderable thanks to the use of a FOAW velocity estimator which allows for higher "control gains" K and B. The FOAW velocity estimation was also tested within the inner motion control loop of the AdmC but did not result in better performance.

B. Performance Characterization

As the interaction forces felt by a patient during robot-assisted therapy are always a combination of the desired dynamics and the apparent device dynamics, it is crucial that a detailed performance characterization be provided for each device and considered during the interpretation of patient assessments. A number of meaningful performance metrics have been proposed in literature for this purpose [19], [20], including maximum velocity/acceleration and inertial ratio, as well as more advanced metrics such as the Z-width.

As an additional metric, the proposed transparency planes capture the dynamics of the interaction induced by the user, rather than relying on a simulation/estimation of the theoretically optimal performance. We scaled the x- and y-axes to the maximal achievable velocity and acceleration (saturation limits). This extends the regression concept proposed in [5], by visualizing the extent to which the implemented controller allows the user to exploit the maximal achievable device dynamics, and complements the information gathered from other haptic performance metrics such as a Z-width plot. R^2 values, maximum and averaged residuals of the fitted transparency planes revealed almost perfect linearity for the ImpC with force feedback and the AdmC. Larger maximum and averaged residuals for the uncontrolled device reflect uncompensated non-linearities of the ReHapticKnob (e.g. play in the gear and elasticity in the transmission), which are not captured by the linear mass-damper model of the transparency planes. As such, transparency planes offer a simple and intuitive visual assessment of the dynamic performance of a haptic display in transparency rendering.

C. Implications for Robot-Assisted Assessment and Therapy

The broad achievable impedance range of the ImpC with force feedback allows the implementation of rehabilitation exercises in which patients actively move the robot (with/without variable resistance/assistance) or in which the robot passively guides the patient's hand. The ability to render both of these exercise modalities has previously been

identified as a requirement [9], [5], [11], [10] and is important (i) for the appropriate training of patients with a wide range of impairments, from completely plegic to mildly impaired and (ii) for robotic assessments, which aim at analyzing the patients' movement abilities without being altered by the device dynamics [4], [5]. This is often achieved through the development of rehabilitation robots with an inherently low-impedance design (small end-effector, transmission and reflected motor inertias) [9], [4], [5], which can in turn limit the output torque required to passively guide the patients' limbs [9]. Rehabilitation devices which can overcome this tradeoff and train in either modality, i.e., devices with a strong actuation unit and a force transducer at the output, are mostly controlled with either an AdmC [2] or an ImpC with force feedback [10]. However, only the implementation and a direct comparison of these two interaction controllers on the same device allowed us to conclude which concept is superior for our application. The tremendous reduction of the apparent impedance during transparency rendering using the ImpC with force feedback is of special interest for the rehabilitation of dexterous hand function, which is based on the training and assessment of fine motor skills. Thanks to the ImpC with force feedback, sharp transitions from low to high impedance could be implemented on the ReHapticKnob to simulate the interaction with virtual objects. Thereby, rich and realistic virtual environments can be rendered in rehabilitation exercises to train functional tasks and ADL such as grasping and manipulation of rigid objects, which has been shown to be beneficial for motor recovery [28].

ACKNOWLEDGMENTS

This work was supported by the NCCR Neuro of the Swiss National Science Foundation and ETH grant CH1-02 09-3.

REFERENCES

[1] J. Mehrholz, A. Hädrich, T. Platz, J. Kugler, and M. Pohl, "Electromechanical and robot-assisted arm training for improving generic activities of daily living, arm function, and arm muscle strength after stroke," *Cochrane Database Syst Rev*, vol. 6, 2012.

[2] R. Colombo, F. Pisano, S. Micera, A. Mazzone, C. Delconte, M. C. Carrozza, P. Dario, and G. Minuco, "Robotic techniques for upper limb evaluation and rehabilitation of stroke patients," *Neural Systems and Rehabilitation Engineering, IEEE Transactions on*, vol. 13, no. 3, pp. 311–324, 2005.

[3] L. Marchal-Crespo and D. Reinkensmeyer, "Review of control strategies for robotic movement training after neurologic injury," *Journal of neuroengineering and rehabilitation*, vol. 6, no. 1, p. 20, 2009.

[4] C. Takahashi, L. Der-Yeghiaian, V. Le, and S. Cramer, "A robotic device for hand motor therapy after stroke," in *Rehabilitation Robotics, 2005. ICORR 2005. 9th International Conference on*, 2005, pp. 17–20.

[5] N. L. Tagliamonte, M. Scorcia, D. Formica, D. Campolo, and E. Guglielmelli, "Effects of impedance reduction of a robot for wrist rehabilitation on human motor strategies in healthy subjects during pointing tasks," *Advanced Robotics*, vol. 25, no. 5, pp. 537–562, 2011.

[6] J.-C. Metzger, O. Lambercy, A. Califfi, F. Conti, and R. Gassert, "Neurocognitive robot-assisted therapy of hand function," *IEEE Transactions on Haptics*, vol. 7, no. 2, pp. 140–149, 2014.

[7] J. Colgate and J. Brown, "Factors affecting the Z-width of a haptic display," in *Proc. IEEE International Conference on Robotics and Automation*, 1994, pp. 3205–3210.

[8] H. I. Krebs, J. J. Palazzolo, L. Dipietro, M. Ferraro, J. Krol, K. Rannekleiv, B. T. Volpe, and N. Hogan, "Rehabilitation robotics: Performance-based progressive robot-assisted therapy," *Autonomous Robots*, vol. 15, no. 1, pp. 7–20, 2003.

[9] A. Gupta and M. K. O'Malley, "Design of a haptic arm exoskeleton for training and rehabilitation," *Mechatronics, IEEE/ASME Transactions on*, vol. 11, no. 3, pp. 280–289, 2006.

[10] J. F. Veneman, R. Ekkelenkamp, R. Kruidhof, F. C. van der Helm, and H. van der Kooij, "A series elastic-and bowden-cable-based actuation system for use as torque actuator in exoskeleton-type robots," *The international journal of robotics research*, vol. 25, no. 3, pp. 261–281, 2006.

[11] H. Vallery, A. Duschau-Wicke, and R. Riener, "Generalized elasticities improve patient-cooperative control of rehabilitation robots," in *Rehabilitation Robotics, 2009. ICORR 2009. IEEE International Conference on*. IEEE, 2009, pp. 535–541.

[12] M. Bouzit, G. Burdea, G. Popescu, and R. Boian, "The rutgers master ii-new design force-feedback glove," *Mechatronics, IEEE/ASME Transactions on*, vol. 7, no. 2, pp. 256–263, 2002.

[13] C. N. Schabowsky, S. B. Godfrey, R. J. Holley, P. S. Lum *et al.*, "Development and pilot testing of hexorr: hand exoskeleton rehabilitation robot," *Journal of neuroengineering and rehabilitation*, vol. 7, no. 1, p. 36, 2010.

[14] J.-C. Metzger, O. Lambercy, D. Chapuis, and R. Gassert, "Design and characterization of the ReHapticKnob, a robot for assessment and therapy of hand function," in *Proc. IEEE/RSJ International Conference on Intelligent Robots and Systems (IROS)*, 2011, pp. 3074–3080.

[15] J.-C. Metzger, O. Lambercy, and R. Gassert, "High-fidelity rendering of virtual objects with the ReHapticKnob – novel avenues in robot-assisted rehabilitation of hand function," *Proc. IEEE Haptics Symposium*, 2012.

[16] C. Carignan and K. Cleary, "Closed-loop force control for haptic simulation of virtual environments," *Haptics-e*, vol. 1, no. 2, pp. 1–14, 2000.

[17] N. Hogan, H. Krebs, B. Rohrer, J. Palazzolo, L. Dipietro, S. Fasoli, J. Stein, R. Hughes, W. Frontera, and D. Lynch, "Motions or muscles? Some behavioral factors underlying robotic assistance of motor recovery," *Journal of Rehabilitation Research and Development*, vol. 43, no. 5, p. 605, 2006.

[18] M. Ueberle and M. Buss, "Control of kinesthetic haptic interfaces," in *Proc. IEEE/RSJ International Conference on Intelligent Robots and Systems (IROS)*, 2004.

[19] V. Hayward and O. Astley, "Performance measures for haptic interfaces," in *Int. Symp. on Robotics Research*, vol. 7, 1996, pp. 195–206.

[20] D. Weir, J. Colgate, and M. Peshkin, "Measuring and increasing Z-width with active electrical damping," in *Proc. Symposium on Haptics*, 2008, pp. 169–175.

[21] T. Massie and J. Salisbury, "The phantom haptic interface: A device for probing virtual objects," in *Proc. of the ASME winter annual meeting, symposium on haptic interfaces for virtual environment and teleoperator systems*, vol. 55, no. 1, 1994, pp. 295–300.

[22] N. Hogan and S. Buerger, "Impedance and interaction control," *Robotics and Automation Handbook*, pp. 19–1, 2005.

[23] E. Faulring, J. Colgate, and M. Peshkin, "The cobotic hand controller: Design, control and performance of a novel haptic display," *The International Journal of Robotics Research*, vol. 25, no. 11, pp. 1099–1119, 2006.

[24] F. Janabi-Sharifi, V. Hayward, and C. Chen, "Discrete-time adaptive windowing for velocity estimation," *IEEE Transactions on Control Systems Technology*, vol. 8, no. 6, pp. 1003–1009, 2000.

[25] W. S. Newman and Y. Zhang, "Stable interaction control and coulomb friction compensation using natural admittance control," *Journal of robotic systems*, vol. 11, no. 1, pp. 3–11, 1994.

[26] E. Colgate and N. Hogan, "The interaction of robots with passive environments: Application to force feedback control," in *Advanced Robotics: 1989*. Springer, 1989, pp. 465–474.

[27] R. Van der Linde, P. Lammertse, E. Frederiksen, and B. Ruiter, "The HapticMaster, a new high-performance haptic interface," in *Proc. Eurohaptics*, 2002, pp. 1–5.

[28] C. J. Winstein, D. K. Rose, S. M. Tan, R. Lewthwaite, H. C. Chui, and S. P. Azen, "A randomized controlled comparison of upper-extremity rehabilitation strategies in acute stroke: a pilot study of immediate and long-term outcomes," *Archives of physical medicine and rehabilitation*, vol. 85, no. 4, pp. 620–628, 2004.